Holographic lithography of periodic two- and three-dimensional microstructures in photoresist SU-8

Toshiaki Kondo, Saulius Juodkazis, Vygantas Mizeikis and Hiroaki Misawa

JST-CREST and Research Institute for Electronic Science, Hokkaido University, N21-W10, CRIS Bldg., Kita-ku, Sapporo 001-0021, Japan

Misawa@es.hokudai.ac.jp

Shigeki Matsuo

Department of Ecosystems Engineering, The University of Tokushima, 2-1 Minamijosanjima, Tokushima 770-8506, Japan

Abstract: Micro-fabrication of periodic structures was performed by holographic lithography technique in SU-8 photoresist using a simple and versatile experimental arrangement based on a diffractive beam-splitter. High-fidelity two- and three-dimensional microstructures fabricated with sub-micrometric resolution in large areas of approximately 1 mm diameter. The structures are potentially usable as elements of micro-fluidic systems (e.g., Brownian ratchets), and templates for photonic crystal devices (e.g., mirrors, collimators, superprisms).

OCIS codes: (220.4000) Microstructure fabrication; (220.4610) Optical fabrication; (160.4670) Optical materials; (160.5470) Polymers;

References and links

1. V. Berger, O. Gauthier-Lafaye, and E. Costard, "Photonic band gaps and holography," J. Appl. Phys. **82**, 60 – 64 (1997).
2. M. Campbell, D. N. Sharp, M. T. Harrison, R. G. Denning, and A. Turberfield, "Fabrication of photonic crystals for the visible spectrum by holographiclithography," Nature **404**, 53 – 56 (2000).
3. T. Kondo, S. Matsuo, S. Juodkazis, and H. Misawa, "A novel femtosecond laser interference technique with diffractive beam splitter for fabrication of three-dimensional photonic crystals," Appl. Phys. Lett. **79**(6), 725–727 (2001).
4. T. Kondo, S. Matsuo, S. Juodkazis, V. Mizeikis, and H. Misawa, "Three-dimensional recording by femtosecond pulses in polymer materials," J. Photopolym. Sci. Tech. **16**, 427–432 (2003).
5. S. Juodkazis, T. Kondo, V. Mizeikis, S. Matsuo, and H. M. andH. Misawa, "Three-dimensional recording by femtosecond pulses in dielectrics," in *Photonics West, Photon Processing in Microelectronics and Photonics II (27-30Jan. 2003, San Jose, U. S. A.) SPIE Proc. 4977*, A. Piqué, K. Sugioka, P. R. Herman, J. Fieret, F. G. B. J. J. Dubikovsky, W. Hoving, K. Washio, D. B. G. andF. Träger, and K. Murakami, eds., 94–107 (2003).
6. A. Chelnokov, S. Rowson, J.-M. Lourtioz, V. Berger, and J.-Y. Courtois, "An optical drill for the fabrication of photonic crystals," Journal of Optics A **1**, L3–L6 (1999).
7. J. H. Moon, S. M. Yang, D. Pine, and W. Chang, "Multiple-exposure holographic lithography with phase shift," Appl. Phys. Lett. **85**, 4184–4186 (2004).
8. H. Su, Y. C. Zhong, X. Wang, X. G. Zheng, J. F. Xu, and H. Z. Wang, "Effects of polarization on laser holography for microstructure fabrication," Phys. Rev. E **67**, 056,619 (2003).
9. S. Matthias and F. Müller, "Asymmetric pores in a silicon membrane acting as massively parallel brownian ratchets," Nature **424**, 53–57 (2003).
10. N. Tétreault, G. von Freymann, M. Deubel, M. H. F. Pérez-Willard, S. John, M. Wegener, and G. A. Ozin, "New route to three-dimensional photonic bandgap materials: silicon double inversion of polymer templates," Adv. Materials **18**, 457–460 (2005).

#71499 - $15.00 USD Received 31 May 2006; revised 10 August 2006; accepted 12 August 2006

11. H. Kosaka, T. Kawashima, A. Tomita, M. Notomi, T. Tamamura, T. Sato, and S. Kawakami, "Superprism phenomena in photonic crystals," Phys. Rev. B **58**, 10,096 – 10,099 (1998).
12. H. Kosaka, T. Kawashima, A. Tomita, M. Notomi, T. Tamamura, T. Sato, and S. Kawakami, "Photonic crystals for micro lightwave circuits using wavelength-dependent angular beam steering," Appl. Phys. Lett **74**, 1370 – 1372 (1999).
13. T. Prasad, V. Colvin, and D. Mittleman, "Superprism phenomenon in three-dimensional macroporous polymer photonic crystals," Phys. Rev. A **67**, 165,103–1/7 (2003).
14. C. Luo, M. Soljacic, and J. Joannopoulos, "Superprism effect based on phase velocities," Opt. Lett. **29**, 745–747 (2004).
15. L. Wu, M. Mazilu, T. Karle, and T. F. Krauss, "Superprism phenomena in planar photonic crystals," IEEE J. Quant. Electron. **38**, 915–918 (2002).
16. A. Maznev, T. Crimmins, and K. Nelson, "How to make femtosecond pulses overlap," Opt. Lett. **23**, 1378 –1380 (1998).
17. T. Kondo, S. Juodkazis, and H. Misawa, "Reduction of capillary force for high aspect-ratio nanofabrication," Appl. Phys. A **81**, 1583–1586 (2005).
18. S. Yang, M. Megens, J. Aizenberg, P. Wiltzius, P. M. Chaikin, and W. B. Russel, "Creating Periodic Three-Dimensional Structures by Multibeam Interference of Visible Laser," Chem. Mater. **14**, 283–2833 (2002).
19. T. Kondo, S. Matsuo, S. Juodkazis, V. Mizeikis, and H. Misawa, "Multiphoton fabrication of periodic structures by multibeam interferenceof femtosecond pulses," Appl. Phys. Lett. **82**(17), 2758–2760 (2003).
20. S. Matsuo, T. Kondo, S. Juodkazis, V. Mizeikis, and H. Misawa, "Fabrication of three-dimensional photonic crystals by femtosecond laserinterference," in *Photonic Bandgap Materials and Devices (Jan. 19-25 2002, San Jose, U. S.A.) SPIE Proc. 4655*, A. Adibi, A. Scherer, and S.-Y. Lin, eds., 327–334 (2002).
21. S. Juodkazis, T. Kondo, V. Mizeikis, S. Matsuo, H. Misawa, E. Vanagas, and I. Kudryashov, "Microfabrication of three-dimensional structures in polymer and glass by femtosecond pulses," in *ROC-Lithuania Bilateral Conf. Optoelectronics & Magnetic Materials (May25-26 2002, Taipei, Taiwan) Proc.*, 27–29 ((preprint: http://arXiv.org/abs/physics/0205025), 2002).
22. S. Juodkazis, T. Kondo, S. Dubikovski, V. Mizeikis, S. Matsuo, and H. Misawa, "Three-dimensional holographic recording in photo-thermo-refractive glass by femtosecond pulses," in *Int. Conf. Advanced Laser Technologies, ALT-2002 (Sept. 15-20 2002, Adelboden,Switzerland) SPIE Proc. 5147*, H. P. Weber, V. I. Konov, and T. Graf, eds., 226 – 235 (2003).
23. J. N. Israelachvili, *Intermolecular and surface forces*, 2nd ed. (Academic Press Ltd., London, 1992).
24. T. Tanaka, M. Morigami, and N. Atoda, "Mechanism of resist pattern collapse during development process," Jpn. J. Appl. Phys. **32**, 6059–6064 (1993).
25. T. Kondo, S. Juodkazis, V. Mizeikis, and H. Misawa, "Three-dimensional high-aspect-ratio recording in resist," J. Non-Crystall. Solids (2005 (in press)).
26. A. Blanco, E. Chomski, S. Grabtchak, M. Ibisate, S. John, S. Leonard, C. Lopez, F. Meseguer, H. Miguez, J. Mondia, G. Ozin, O. Toader, and H. van Driel, "Large-scale synthesis of a silicon photonic crystal with a complete three-dimensional bandgap near 1.5 micrometres," Nature **405**, 437–40 (2000).
27. Y. V. Miklyaev, D. C. Meisel, A. Blanco, G. von Freymann, K. Busch, W. Koch, C. Enkrich, M. Deubel, and M. Wegener, "Three-dimensional face-centered-cubic photonic crystal templates by laser holography: fabrication, optical characterization, and band-structure calculations," Appl. Phys. Lett. **82**, 1284–1286 (2003).

1. Introduction

Interest in three-dimensional (3D) maskless micro- and nano-processing of materials is fueled by the need of novel photonic crystal, plasmonic, near-field, and micro-fluidic devices for applications in various fields, like micro electro-mechanical systems (MEMS). While the systems' miniaturization yields enhanced integration and improved functionality, their fabrication in 3D becomes increasingly more costly and tedious using traditional approaches, like planar semiconductor processing techniques. To ensure high fabrication throughput at low cost, fabrication methods natively suitable for 3D fabrication must be developed. In this respect one of the highly useful techniques is lithography in the bulk of photosensitive materials based on multi-photon exposure to the periodic patterns created by the interference of several coherent laser beams [1, 2, 3]. The interfering fields are obtained from a single laser beam, split into multiple components, and the method is similar to recording of holograms. Various periodic 3D patterns can be created by changing the number of interfering beams and their directions, amplitudes, phases and polarizations [4, 5, 6, 7, 8]. The structures recorded by holographic lithography can be used as building elements of larger micro-fluidic systems, for example Brownian ratch-

#71499 - $15.00 USD Received 31 May 2006; revised 10 August 2006; accepted 12 August 2006

ets [9], templates of photonic crystals to be infiltrated by high refractive index materials [10], photonic crystal superprisms [11, 12, 13, 14, 15], etc. Previously we have demonstrated a simple and versatile implementation of holographic lithography based on the diffractive beam-splitter (DBS) [3, 4], which allowed to obtain any number of coherent beams and achieve their perfect spatio-temporal overlap using a few optical elements. This method is especially convenient when exposure is done using ultrashort laser pulses. Ultrafast excitation allows one to induce non-linear absorption in transparent materials at moderate average power levels. The nonlinear nature of photoexcitation allows fabrication of smaller features and deeper penetration into the material than would be possible in a linear regime where materials are uniformly absorbing. The nonlinearity also helps reduce the undesirable exposure to the spatially uniform "dc" component of the interference pattern (due to non-optimum intensity ratios and polarizations of the beams). However, holographic lithography with ultrashort pulses imposes additional requirements on the spatio-temporal pulse overlap. For example, pulses with temporal length of 100 fs, typically achievable with Ti:Sapphire lasers, have a spatial length of 30 μm, which sets the maximum allowable optical path difference between the beams. With these restrictions, it is impossible to employ Mach-Zehnder or Lloyds mirror optical schemes, used for holographic lithography with continuous-wave or long-pulse sources. The use of DBS automatically ensures the uniformity of optical paths for all beams without the need for multiple optical delay lines. Moreover, beams passed through the DBS, which essentially are diffracted orders of a grating, deliver pulses with tilted wave fronts. The tilt ensures that pulses converging on the sample at a large mutual angle are simultaneous and can interfere in the entire irradiated area [16].

Our previous work [3, 4] mainly concentrated on the recording of 3D periodic microstructures in negative photoresist SU-8 using the DBS-based optical scheme and a femtosecond Ti:Sapphire laser. The best quality structures reported therein were recorded using frequency-doubled pulses having central wavelength of 400 nm. According to our experience, in these circumstances a strong cross-linking in SU-8 is induced, which produces large, strongly overlapping features. This can be tentatively explained by the spectral proximity and partial overlap of the broadband laser pulses and the spectral region of linear optical absorption, which in SU-8 occurs at wavelengths shorter than about 360 nm. An additional exposure may be induced due to the generation and absorption of broadband secondary radiation (white-light continuum and fluorescence). Under repeated excitation, accumulation of thermal effects following each incidence of the laser pulses may also lead to cross-linking. Altogether these mechanisms may result in what can be termed as a quasi-linear, non-local absorption in SU-8. Therefore, our 3D structures fabricated earlier at 400 nm wavelength always consisted of well-connected SU-8 regions and were mechanically stable. The unsuccessful samples mostly resulted from too much cross-linking, which produced structures having low air-filling fraction, and large features, or a uniform SU-8. On the other hand, exposure by the laser pulses of the fundamental wavelength of a Ti:Sapphire laser (800 nm) always exhibited a cross-linking at well-localized locations, with clear intensity threshold, and feature size strongly dependent on the exposure, in compliance with a predominantly nonlinear absorption. Absence of additional exposure mechanisms at this wavelength suggests that holographic fabrication can be performed more accurately and is easier to control via optical exposure. In practice it was easier to achieve higher air-filling fraction and obtain well-defined features at this wavelength. However, there was a large percentage of unsuccessful samples in which features tended to be separated from each other and deformed, leading to the loss of short-range and long-range periodicity, and structural distortions (see Figs. 4 and 5 in Ref. [4] for illustration). Later, we have found that these distortions are mainly due to capillary forces acting on thin SU-8 features during the drying of isopropanol, used for rinsing of the samples after the development [17].

This study is aimed at DBS-based holographic fabrication of well-ordered, mechanically

#71499 - $15.00 USD Received 31 May 2006; revised 10 August 2006; accepted 12 August 2006

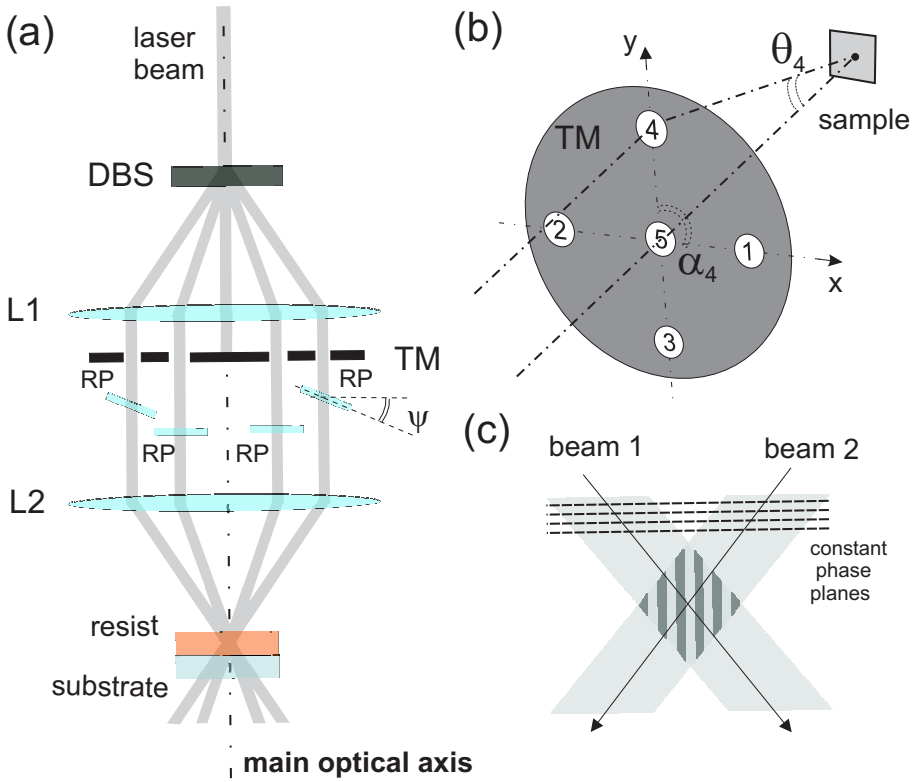

Fig. 1. Holographic 3D recording using diffractive beam-splitter (a), description of the set of beams used for recording, beams selected by the holes in the amplitude mask are labeled by numbers (b), two pulses with tilted wavefronts converge with negligible optical path difference and interfere in the entire region of their spatial overlap (c).

stable periodic structures using femtosecond pulses with central wavelength of 800 nm, and at minimization of structural distortions in these structures during their drying. Without access to a super-critical drying (SCD), known to be the most efficient way to eliminate the action of capillary forces [18], we have used a simple alternative method to alleviate the distortions. By rinsing the samples in water after isopropanol, capillary forces were reduced significantly due to the hydrophobic nature of the SU-8 surface.

2. Experimental details

2.1. Holographic lithography and its experimental implementation

The principle of holographic lithography is schematically illustrated in Fig. 1(a). The optical setup was described in detail earlier [3, 19]. The laser beam for the fabrication is derived from a femtosecond Ti:Sapphire laser system (not shown), which produces 150 fs duration pulses centered at the 800 nm wavelength at a repetition rate of 1 kHz. Excitation by the femtosecond pulses provides peak power levels higher than would be achievable with longer (picosecond or nanosecond) pulses, enabling one to induce non-linear absorption at low average power levels in various materials, which are optically transparent in the linear regime. The laser beam is passed through the DBS, which can be interpreted as a stack of two-dimensional (2D) diffrac-

#71499 - $15.00 USD Received 31 May 2006; revised 10 August 2006; accepted 12 August 2006

tion gratings having different groove orientations. The first grating splits the beam into the transmitted (zero-order) and diffracted (first and higher order) components. These components subsequently pass through other gratings where they again diffract into other directions. As a result a set of multiple beams propagating along the directions diverging symmetrically around that of the initial beam is obtained. DBS actually uses a single plate with recorded transfer functions of several gratings. The beams needed for the creation of the desired interference pattern are selected using a transmission mask TM. The unmasked beams are collimated and converged to overlap on the sample using a pair of lenses L1 and L2.

Period and symmetry of the point lattice of the periodic interference pattern is determined by the set of selected beams and their relative phases. The set of n beams can be described as illustrated schematically in Fig. 1(b). The i-th beam from the set is described by the azimuthal and radial positions in the plane of the mask; these angles are denoted α_i and θ_i, respectively. Phases of the beams, denoted as ϕ_i can be controlled using adjustable retarders RP, which are glass plates inserted into beams' paths at an angle ψ as illustrated in Fig. 1(a). Thus, n recording beams can be described using notation of the form $[\alpha_1, \theta_1\, \phi_1]$, $[\alpha_2, \theta_2\, , \phi_2]$,...$[\alpha_n, \theta_n\, \phi_n]$.

The light intensity distribution $I(\mathbf{r})$ at the focus due to interference of multiple beams can be approximated as a superposition of plane waves. For beams converging at moderate mutual angles, at which longitudinal components of the electric field parallel to the main optical axis of the system are negligible, the spatially-modulated intensity $I(\mathbf{r})$ is expressed as:

$$I(\mathbf{r}) = \sum_{n,m} \mathbf{E_n} e^{-i(\mathbf{k_n}\cdot\mathbf{r}+\phi_n)} \cdot \mathbf{E_m^*} e^{i(\mathbf{k_m}\cdot\mathbf{r}+\phi_m)}, \tag{1}$$

where $\mathbf{E}$ is the complex E-field vector, $\mathbf{r}$ is the coordinate vector, $\mathbf{k}$ is the wave-vector, and $n = m$ is the number of interfering beams. The phase differences of the beams are denoted as $\phi_{n,m}$. Controlling the phases of the beams allows for a fine tuning of the interference patterns [20, 21, 22].

The use of DBS is particularly convenient for experiments with ultrafast lasers because it produces so-called tilted pulses whose wave-front is perpendicular to the main optical axis of the system [16], as illustrated schematically in Fig. 1(c). The tilt ensures a perfect temporal overlap across the entire cross-sectional area of the beams. Furthermore, well-known relationship between the angle of diffraction and the light wavelength ensures that identical interference patterns are obtained regardless of the wavelength. Thus, well-defined patterns can be obtained even with broadband (for example ultrashort pulses) or multicolor laser beams [1].

2.2. Samples and their processing

The interference pattern was recorded in films of SU-8, a commercially available ultra-thick negative polymeric photoresist, which in the linear regime is optically transparent at the 800 nm wavelength. At an appropriately chosen laser pulse intensity, nonlinear two-photon absorption (TPA) or multi-photon absorption (MPA) is induced selectively in the spatial regions where local power density exceeds a characteristic threshold value. Optical exposure in these regions leads to polymer cross-linking during the subsequent post-exposure bake, rendering them insoluble in the developer, which removes only the unexposed regions. As a result, a replica of the original interference pattern featuring a cross-connected 3D network of solid SU-8 features in air is obtained. SU-8 is designed for lithographic fabrication of micromechanical systems and is therefore robust mechanically and chemically. As-fabricated, SU-8 provides a stable platform for micromechanical systems. Its refractive index ($n \approx 1.6$) is considerably higher than that of air ($n = 1$), which is sufficient for some applications which do not require complete photonic band-gap (PBG). Whenever a complete PBG is needed, periodic SU-8 structures can be considered as photonic crystal templates suitable for infiltration with other materials having higher refractive index.

#71499 - $15.00 USD Received 31 May 2006; revised 10 August 2006; accepted 12 August 2006

In preparing the samples, films of SU-8 from Microchem Co. were spin-coated to the thickness of $2-25\,\mu$m, depending on the desired height of the structure, on the cover glass substrates. The samples were soft-baked, and after the exposure post-baked according to the manufacturers' recommendations. SU-8 developer from Microchem was used for development of the samples. The final step of the standard SU-8 processing is rinse in isopropanol after the development. A considerable structural damage may result from capillary drainage of the rinsing liquid during the drying. Taking as an example a pair of solid cylindrical rods with radii R, separated by the distance l, the capillary force between them can be expressed as $F = 2\pi h\gamma\cos\theta(1+D/d)$, where h is the height of the rods, γ is the surface tension, θ is the contact angle, $D = l-2R$ is the gap between the two cylinders, and d is the projection distance between the points of the liquid/cylinder contact and the edge of the cylinder ($d \to 0$, $\theta = \pi/2$ for non-wetting, $d \to R$, $\theta = \pi/2$ for full wetting conditions) [23]. When distance between the features decreases, the capillary force becomes stronger. Critical Young's modulus for the cylinders to withstand the capillary drainage is given by [24]:

$$E_{cr} = \frac{24\gamma h^4}{(2R)^3 D^2}, \tag{2}$$

Capillary force exceeding the Young modulus may damage the features. Young modulus of SU-8 features depends on the degree of their cross-linking, which is dependent on the exposure dose and post-exposure treatment conditions.

Drying in a super-critical liquid eliminates the surface tension $\gamma \to 0$ and helps to preserve the structure [18]. In the absence of super-critical drying facility, the destructiveness of capillary forces was reduced by decreasing the surface tension, or the contact angle during the final rinse of the samples. Isopropanol, which is the standard SU-8 rinsing agent, has surface tension of $\gamma = 21.8\,\text{mJ/cm}^2$ and contact angle of $\theta = 20^0$, i.e., it is strongly wetting the SU-8 surface. Water has a higher surface tension $\gamma = 72\,\text{mJ/cm}^2$, but since SU-8 surface is hydrophobic, with contact angle $\theta = 81^0$, the capillary force exerted by water is about twice smaller than that by isopropanol, which is water soluble. Therefore, final rinse in the water was used for all fabricated samples, and has greatly improved their survival rate. More details about this technique can be found elsewhere [17, 25].

3. Results and discussion

It can be shown using Eq. (1) that recording of 2D interference patterns needs at least three laser beams converging at non-zero angles with respect to the main optical axis of the system (see Fig. 1 (a,b)). Period of the pattern is controlled by the mutual angles of the beams. For 3D patterns, at least four beams are required. With the simple setup used in our work changing the number and mutual alignment of the interfering beams is very easy, and basically involves changing or repositioning the amplitude mask. Thus, as far as the experimental implementation is concerned, there are no principal experimental differences between fabrication of 2D and 3D structures. 2D structures are easier to visualize using optical or scanning electron microscopy (SEM) than their 3D counterparts. Visualization plays important role in assessing the quality of structures and their correspondence to the original interference pattern calculated according to Eq. (1). Non-destructive visualization of internal regions of 3D structures is difficult and their structural properties can be only assessed by examining the topology of the patterns seen on their outer surfaces. Below we describe fabrication and characteristics of several 2D and 3D structures.

#71499 - $15.00 USD Received 31 May 2006; revised 10 August 2006; accepted 12 August 2006

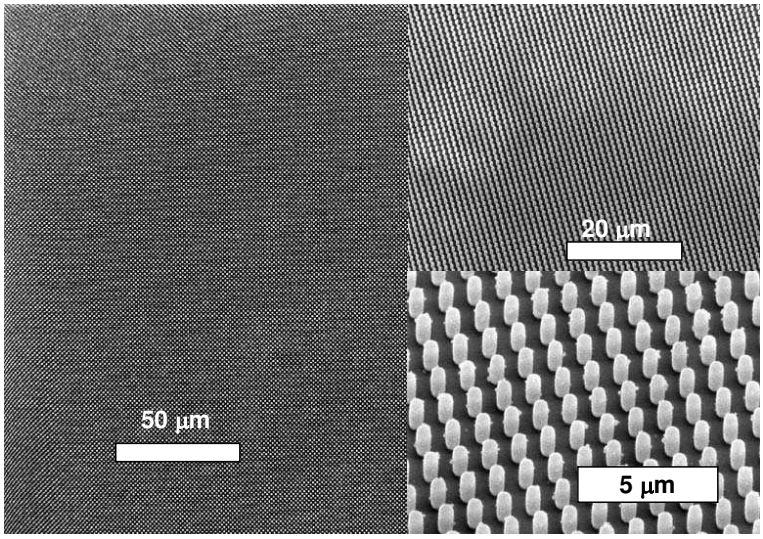

Fig. 2. SEM images of two-dimensional square pattern of circular SU-8 pillars at different magnification.

3.1. Two-dimensional patterns

Figure 2 demonstrates the structure consisting of circular rods arranged into a square lattice. The four recording beams have same phase and converge on the sample symmetrically from the corners of a square. Using the notation introduced earlier, such arrangement can be described as $\left[0^0, 34^0\right], \left[90^0, 34^0\right], \left[180^0, 34^0\right], \left[270^0, 34^0\right]$ (the phase, which is the same for all beams is omitted here). The moderate radial angle, $\theta = 34^0$, ensures a negligible longitudinal component of the optical field in accordance with Eq. (1).

The period of the square lattice, $a = 1.05\,\mu$m, is close to the value of $1.02\,\mu$m obtained from the pattern calculated according to Eq. (1). The rods in the fabricated structure have diameter $d = 0.43\,\mu$m and height $h = 1.3\,\mu$m. The latter two parameters depend on the intensity of recording beams and the thickness of SU-8 film. During the recording, the sample was exposed for 1 min. to pulses of 20 μJ energy at 1 kHz repetition rate. The structure produced during this relatively short time exhibits a high degree of uniformity of the individual rods' shape and size across a large area having the diameter of about 1 mm. High fidelity of the pattern can be attributed to the fact uniform intensity distribution, achieved by utilizing the central part of a strongly expanded Gaussian beam.

Figure 3 illustrates the role of phase control in recording of 2D structures. The phase shifts are introduced by slightly tilting the phase retarder plates shown schematically in Fig. 1. The adjustment involved phase shift between diagonally-paired beams of the arrangement described earlier, by the amount $\pi/2$. This configuration can be described as $\left[0^0, 20.4^0\, 0\right]$, $\left[90^0, 20.4^0, \pi/2\right]$, $\left[180^0, 20.4^0, 0\right]$, $\left[270^0, 20.4^0, \pi/2\right]$. For easier distinction between spatial angles and phases, the former are given in degrees, while the latter are given in radians. Comparison between the 2D intensity patterns with and without the phase shifts is given in Fig. 3(a,c), which shows experimental patterns recorded by a CCD camera. As can be seen, the phase shift inverts square pattern and rotates it by the angle $\pi/4$. SEM images of these patterns were recorded in SU-8 are shown in Fig. 3(b,d). For uniform phases (b), square lattice has the period of $1.7\,\mu$m, and the average rod diameter of $1.2\,\mu$m. For phase-shifted configuration, the lattice period is $1.6\,\mu$m

#71499 - $15.00 USD Received 31 May 2006; revised 10 August 2006; accepted 12 August 2006

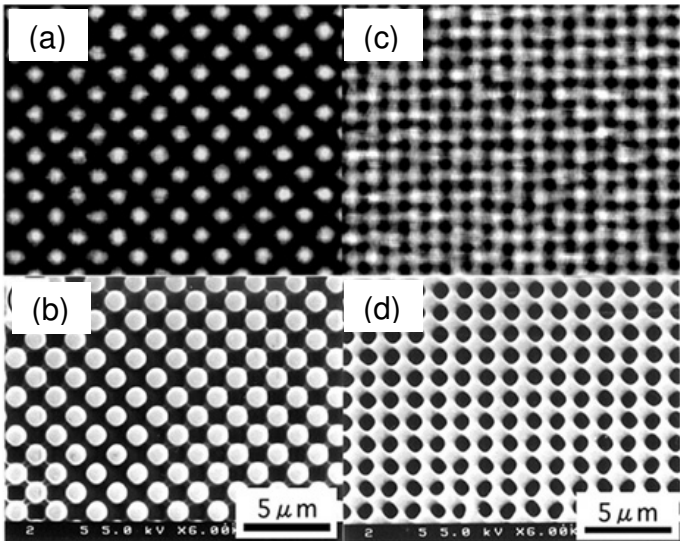

Fig. 3. Four-beam interference patterns for uniform-phase $[0^0, 20.4^0]$, $[90^0, 20.4^0]$, $[180^0, 20.4^0]$, $[270^0, 20.4^0]$ and phase-shifted $[0^0, 20.4^0, 0]$, $[90^0, 20.4^0, \pi/2]$, $[180^0, 20.4^0, 0]$, $[270^0, 20.4^0, \pi/2]$ configurations, (a,b) and (c,d), respectively. The images in (a) and (c) are intensity patterns visualized by a CCD camera, while images in (b) and (d) are SEM micro-graphs of samples recorded in SU-8 via two-photon absorption.

and the average diameter of the slightly elongated holes is $0.9\,\mu$m.

3.2. Three-dimensional patterns

Recording of 3D structures requires only a minor change in the beam arrangement. We have used the four-beam configuration without phase shift $[0^0, 34^0]$, $[90^0, 34^0]$, $[180^0, 34^0]$, $[270^0, 28^0]$, a slightly asymmetrical version of the arrangement used in the recording of 2D structures. The asymmetry leads to a slight tilt of the the unit cell of the structure with respect to the main optical axis. The corresponding 3D intensity distribution is shown in Fig. 4(a). This pattern was recorded in a 25 μm thick SU-8 film. We stress here that collapse and critical distortions of these 3D structures was successfully prevented only when the modified post-development procedure described in Section 2.2 was used. The top view of the structure is shown in Fig. 4(b). For better comparison with theoretical result in Fig. 4(a), calculated 2D intensity map at the plane coincident with the sample's surface is shown superimposed on the SEM image. The central part of experimental and calculated images clearly exhibit square patterns of rods with diameter of about $0.9\,\mu$m and period of about $1.0\,\mu$m. Figure 4(c) shows large-scale view of the sample's surface which exhibits a secondary modulation with period of about $4.2\,\mu$m due to the tilt of the unit cell. The image also reveals uniformity of the structure within large area extending over hundreds of micrometers. The total area of this, as well as other samples was close to 1 mm in diameter. Figure 5 demonstrates good agreement between the sample's topology and the calculated field patterns on the planes coinciding with three facets of the sample open for inspection by SEM. These patterns illustrate strong elongation of the structure in direction of the main optical axis of the setup. The structural elements, seen as rods forming the square lattice in the inset to Fig. 4(b), have length of about $11.5\,\mu$m; lattice period along this direction is also similar.

#71499 - $15.00 USD Received 31 May 2006; revised 10 August 2006; accepted 12 August 2006

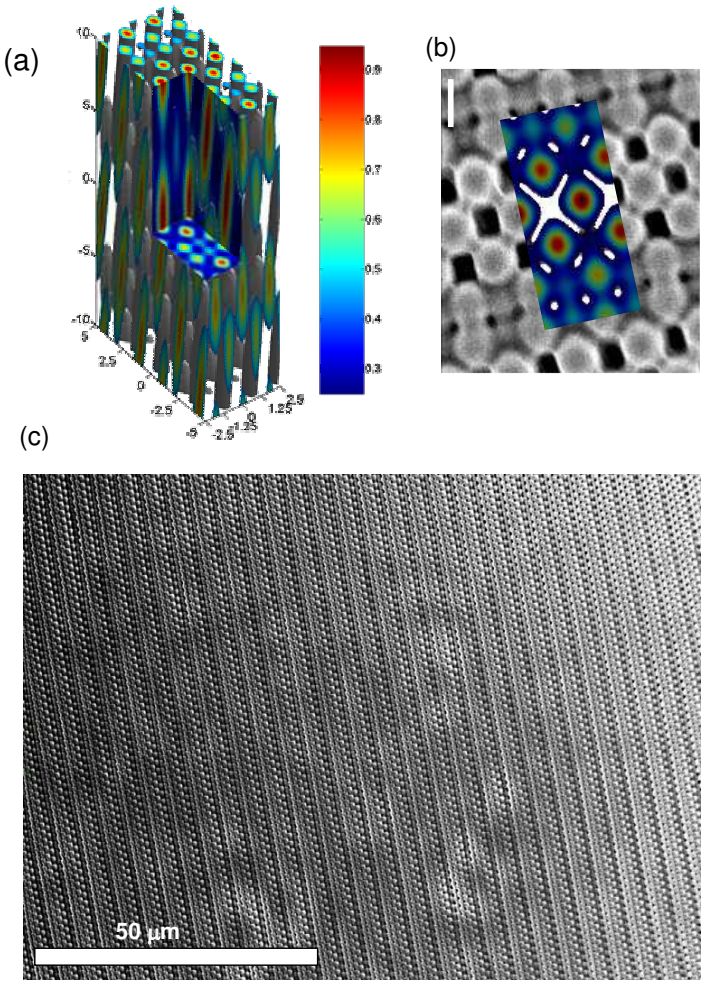

Fig. 4. (a) calculated 3D intensity distribution resulting from the $[0^0, 34^0]$, $[90^0, 34^0]$, $[180^0, 34^0]$, $[270^0, 28^0]$ beam arrangement, (b) calculated intensity distribution corresponding to the 2D plane coincident with the sample's surface superimposed on the SEM image of the actual sample, (c) large-scale SEM image of the sample, illustrating its uniformity.

Careful examination of the sample and the calculated field patterns in Figures 4 and 5 reveal that its point lattice has a lattice symmetry that can be informally described as a body-centered tetragonal (bct), and the dielectric "atoms" are ellipsoids elongated in the direction of the main optical axis of the recording setup. Periodic structures having body-centered cubic (bcc) and bct lattice symmetries can only open photonic band-gaps at large refractive index contrast approaching 3.5 to 1 [26]. Since refractive index of SU-8 is about 1.6 (at infrared wavelengths), index contrast in our structures is 1.6 to 1, and photonic band-gap can not be opened. Elongation of the bct unit cell, resulting from the moderate beam convergence angles, creates a strong anisotropy in the periodicity of the 3D structures, with slowest variations along the direction parallel to the main optical axis of the setup. This anisotropy further diminishes the likelihood

#71499 - $15.00 USD Received 31 May 2006; revised 10 August 2006; accepted 12 August 2006

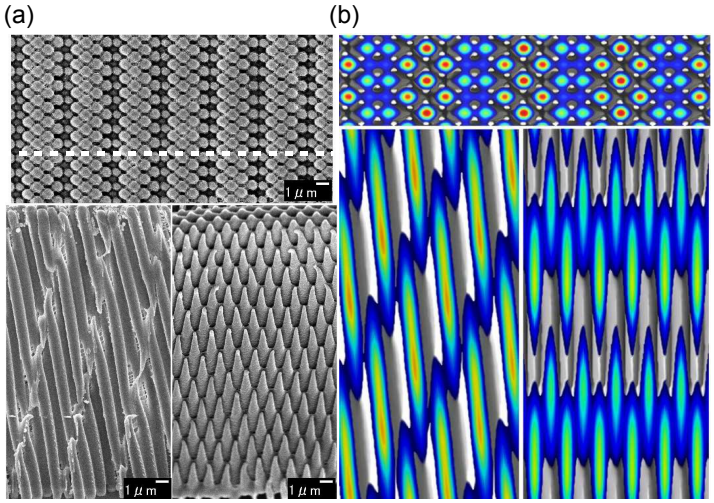

Fig. 5. (a) SEM images of the sample shown in the previous figure, in the top image the white line shows the orientation of the cleaving plane, the bottom-left image shows the portion of the cleaved plane at the middle depth, far from top and bottom surfaces of the sample, the bottom-right image shows the same plane near the top surface, (b) intensity distribution on the planes corresponding to those in (b), calculated from Eq. (1).

of PBG. Reducing the anisotropy toward the cubic unit cell would require to increase mutual angles of the beams. They can be increased by using sharper focusing of the beams on the sample (at the expense of the fabricated area). To overcome the critical incidence angle at the air-sample interface, a specially constructed prism can be employed for coupling of the beams into the sample (at the expense of the flexibility, since different sets of the beams would require prisms with different geometries). Such coupling technique has indeed allowed holographic fabrication of structures having face-centered cubic (fcc) lattice [27].

It can be demonstrated, that a simple modification of the participating beams' number and phases can transform the symmetry of the interference pattern into what can be informally envisioned as face-centered tetragonal (fct) point lattice. Face-centered lattices are known to have robust photonic band gap properties, especially in the case of fcc symmetry. Practical fabrication of these structures using a DBS-based optical setup will be reported elsewhere. Nevertheless, even the anisotropic bct structures fabricated in this work should exhibit photonic stop-gaps, or forbidden frequency ranges existing only along certain directions. Their shorter lattice period is of the order of $1-2\,\mu$m, while the longer lattice period is from few to few tens of micrometers. Therefore, the expected wavelengths of photonic stop-gaps are in the range of about $2-5\,\mu$m and $10-30\,\mu$m along the directions parallel and perpendicular to the surface of the SU-8 film. In these spectral ranges, signatures of vibrational and rotational degrees of freedom of organic molecules are often observed. Structures similar to those fabricated in our work, may be usable for monitoring these degrees of freedom, for instance in photonic crystal environmental sensing applications. For other applications, aimed at exploiting superprism or beam collimation effects [11, 12, 13, 14, 15], existence of photonic stop-gaps is sufficient. Spectral width of the stop-gaps can be enlarged, or their transformation to complete band-gaps can be achieved after the enhancement of their refractive index during subsequent infiltration by other, high-index materials. Infiltration technique allowing to transform low-index SU-8 structures into high-index silicon structures has already been reported [10].

#71499 - $15.00 USD Received 31 May 2006; revised 10 August 2006; accepted 12 August 2006

4. Conclusions

We have microfabricated periodic dielectric microstructures in photoresist SU-8 using a simple and versatile implementation of holographic lithography, and a modified post-processing of samples, aimed at preventing their structural distortions. Various 2D and 3D structures were selected for the fabrication *in situ*, and fabricated using nearly-perfectly synchronized, multiple interfering laser pulses in their entire area of spatial overlap, close to 1 mm in diameter, and comprising large numbers of uniform submicrometric-sized features. Good structural quality and periodicity was assesed by SEM inspection. The structures fabricated in SU-8 are chemically and mechanically stable and are potentially usable as elements of micro-fluidic, micromechanical or photonic crystal devices.

#71499 - $15.00 USD Received 31 May 2006; revised 10 August 2006; accepted 12 August 2006